This paper appears in Medical & Biological Engineering & Computing, 2016.
DOI: 10.1007/s11517-016-1599-1

A Data-Driven Soft Sensor for Needle Deflection in Heterogeneous Tissue using Just-in-Time Modelling

Carlos Rossa, Thomas Lehmann, Ronald Sloboda, Nawaid Usmani, and Mahdi Tavakoli

***Abstract*—Global modelling has traditionally been the approach taken to estimate needle deflection in soft tissue. In this paper, we propose a new method based on local data-driven modelling of needle deflection. External measurements of needle-tissue interactions are collected from several insertions in *ex-vivo* tissue to form a cloud of data. Inputs to the system are the needle insertion depth, axial rotations, and the forces and torques measured at the needle base by a force sensor. When a new insertion is performed, the Just-in-Time (JIT) learning method estimates the model outputs given the current inputs to the needle-tissue system and the historical database. The query is compared to every observation in the database and is given weights according to some similarity criteria. Only a subset of historical data that is most relevant to the query is selected and a local linear model is fit to the selected points to estimate the query output. The model outputs the 3D deflection of the needle tip and the needle insertion force. The proposed approach is validated in ex-vivo multi-layered biological tissue in different needle insertion scenarios. Experimental results in 5 different case studies indicate an accuracy in predicting needle deflection of 0.81 mm and 1.24 mm in the horizontal and vertical planes, respectively, and an accuracy of 0.5 N in predicting the needle insertion force over 216 needle insertions.**

I. Introduction

MINIMALLY invasive percutaneous needle insertion has gained increasing attention over the past few years and has become part of routine clinical practice for tissue sampling, pinpoint drug delivery, permanent brachytherapy, radiofrequency and microwave ablation of liver, lung, and kidney, and regional anaesthesia. The success of these procedures heavily relies on accurate needle placement within an inner body target location. During needle insertion, however, complications arising from needle-tissue interaction cause the needle to deviate from a desired trajectory and deflect away from the target [1–4]. Inaccurate needle placement can compromise the effectiveness of the treatment and lead to significant side effects for the patient.

Typically, solutions to predict and correct the needle targeting errors are based on developing ultrasound image guided strategies or in modelling needle-tissue interaction. The former is challenging since in addition to having a very narrow field of view, ultrasound images contain artifacts that are hard to interpret and distinguish from targets. In addition, the ultrasound probe must move in synchrony with the needle, which can result in unwanted deformation of surrounding tissue and displacement of the target location [5]. The latter often relies on mechanical properties of the tissue.

A variety of needle-tissue interaction models have been developed in order to predict needle deflection and allow for correction of needle tip trajectory while avoid withdrawing and reinserting the needle. Essentially, bevelled-tip needles can be described as following a circular path during insertion whose curvature can be empirically determined for a given tissue [6]. In such models, the tissue is assumed to be stiff relative to the needle as tissue displacement would result in deviations of the needle from the predicted trajectory. In practice, however, this assumption does not hold since the needle deflects and compresses the surrounding tissue, which in turn applies forces to the needle resulting in variation in the curvature.

To account for the fact that needle deflection and tissue deformation are coupled effects and influence each other, mechanics-based and finite element models have been later introduced. In these methods, different needle-tissue contact force profiles are assumed such as constant distributed or concentrated loads along the needle shaft [7], or having linear dependence on the magnitude of local tissue deformation [8, 9]. Finite element methods have also been proposed to account for the effects of needle manipulation and other steering manoeuvres [10, 11]. These physical models require as input the mechanical properties of the tissue, which are difficult to obtain for needles inserted in biological tissue in operating room conditions. In addition, most models can only account for a fixed set of model parameters, which must be re-evaluated for different patients and model inputs. For these reasons, tissue parameters such as Young's modulus, tissue cutting force and stiffness are either assumed to be constant throughout the insertion, or approximated by a series of different local finite homogeneous models of tissue [12].

In order to account for tissue heterogeneity, adaptive models can be considered. Our recent work in [13, 14] outlined a needle deflection model that adaptively updates the needle-tissue cutting force as the needle is inserted. However, the tissue Young's modulus is nevertheless assumed to be constant and the model is limited to planar needle deflection. Along the same line, [15] proposes a method to update the needle curvature used in an online steering controller. In addition to tissue heterogeneity, neither adaptive nor deterministic models can account for other factors that can influence needle deflection such as local tracks in the tissue, tissue anisotropy, and needle buckling. An alternative approach to account for these

This work was supported by the Natural Sciences and Engineering Research Council (NSERC) of Canada under grant CHRP 446520, the Canadian Institutes of Health Research (CIHR) under grant CPG 127768, and by the Alberta Innovates - Health Solutions (AIHS) under grant CRIO 201201232.

Carlos Rossa, Thomas Lehmann, and Mahdi Tavakoli are with the Department of Electrical and Computer Engineering, University of Alberta, AB, Canada T6G 2V4. E-mail: rossa@ualberta.ca; lehmann@ualberta.ca; madhi.tavakoli@ualberta.ca.

Ron Sloboda and Nawaid Usmani are with the Cross Cancer Institute and the Department of Oncology, University of Alberta, Edmonton, AB, Canada T6G 1Z2. E-mail: {ron.sloboda, nawaid.usmani}@albertahealthservices.ca.

uncertainties is to develop data-based methods to build a model from empirical observations of needle-tissue interactions. Such models can be a valuable solution to estimate the system output without deep understanding of system physics.

Traditional data-based modelling methods such as neural networks and fuzzy set, among other nonlinear parametric models, are based on global approaches i.e., data is fit to represent an entire process [16]. This approach often suffers from limitations due to the non-convex nature of the optimization problem, making it difficult to specify the model structure that holds true when the dynamical behaviour is shifted away from its nominal operating range. On the other hand, the idea of local modelling has been introduced to solve this fundamental limitation by approximating a non-linear system with a set of relatively simple local models that are only valid in a constrained operating range.

In this paper we propose a new method to estimate needle tip deflection during insertion suitable for non-homogeneous and multilayered tissue. The needle insertion process is broken down into small multiple regions, each of which is represented by a local linear model valid only in that region. Each data sample then corresponds to an observation of the needle-tissue state at a particular instant in time, rather than considering the entire needle insertion as a single data sample. Thereby, local non-linearities and other uncertainties present in the needle-tissue interaction can be captured. To this end, we used a modified version of the Just-in-Time (JIT) learning method [17]. In this approach when a new input is available to the system (query) it is compared to a database (see Fig. 1). The database is formed by several observations of input-output cause and effect. Only a subset of historical data that is most relevant to the query is selected according to a number of similarity criteria and weighting functions. The similarity criteria quantify how close each data sample is to the query whereas the weighting function assigns weights to the most similar samples. Once the subset of data is selected, a local linear model is fit to the selected points and the system output can be determined. Upon update of the input, the local model is discarded and the process is repeated around the new operating point. The result is a fast model that changes from query to query.

A database was constructed from insertions performed in *ex-vivo* biological tissue. Inputs to the model are the needle insertion depth, the needle axial rotations, and the forces and torques measured at the needle base by a force sensor. The model outputs the needle tip deflection in the vertical and horizontal plane and the needle insertion force (that can be used for developing a haptic simulator for needle insertion). The paper is structured as follows. Section II-A motivates the choice for the model inputs and how each of them influences needle deflection. In Section II-B the JIT model is devised to relate the model inputs to the outputs based on a historical database. The data collection protocol for *ex-vivo* needle insertions is presented in Section III. Experimental results for over 216 needle insertions in phantom tissue in 5 different case studies reported in Section III-B show an accuracy in predicting needle deflection of 0.81 mm and 1.24 mm in the horizontal and vertical planes, respectively. Recommendations for data-driven modelling and potential applications of the proposed method conclude the paper.

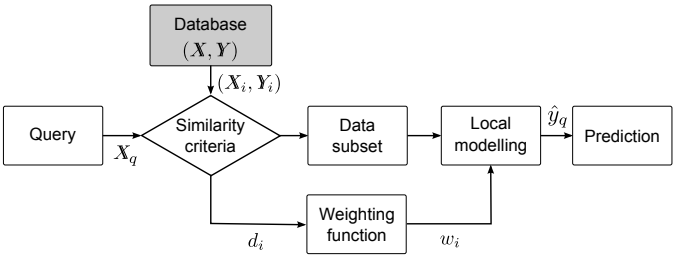

Fig. 1. Work flow of the Just-in-Time modelling approach. The query $\mathbb{X}_q$ is compared to the samples stored in the database $(\mathbb{X}, \mathbb{Y})$ according to some similarity measure d_i. Next, weights w_i are assigned to relevant samples and a local model is built in order to predict the system output $\hat{y}_q$ for the currently query.

II. Methods

A. Needle-tissue Interaction

Before addressing the data-driven model, let us first define the measurable needle insertion parameters that influence the needle deflection and that can be used as model input. Fig. 2 schematically depicts a bevel-tipped needle inserted in soft tissue. u_y and u_x denote the deflection of the needle tip in the (y,z) and (x,z) planes, which will henceforth be referred to as in-plane and out-of-plane deflections, respectively. As the needle tip advances and cuts through tissue, an imbalance of forces is developed at the needle tip leading the needle to deviate from a straight trajectory. The deflected needle shaft compresses the immediately surrounding tissue, which in turn applies forces to the needle. Several factors influence the magnitude and direction of those forces that, for a given needle, can be classified into two main categories i.e., insertion profile specific parameters, and tissue-specific characteristics, as detailed below.

Insertion profile specific parameters include the depth to which the needle is inserted, the needle insertion velocity and the angular position of the bevel angle during insertion.

Insertion depth (d) : Needle deflection increases as the tip advances further into tissue. Hence, the depth to which the needle is inserted is a key factor that determines the amount of observed deflection [6, 9, 18].

Bevel orientation : As the force applied at the needle tip is normal to the bevel angle, changing the orientation of the bevel by rotating the needle base axially brings the needle to deflect in a different direction [9, 13, 19]. A proper combination of needle insertion depth and bevel angle orientation is typically used in robotic assisted needle insertion to force the needle tip to follow a desired trajectory. Throughout this paper, we will only consider axial rotations of 180 degrees, which allows to simply quantify the needle rotation by the distance θ_r from the current needle insertion depth to the r^{th} depth at which the needle is rotated.

Needle insertion velocity (v) : Considering the tissue as a viscoelastic medium, the needle insertion velocity will increase the frictional forces between the needle and tissue and affect the needle insertion force [9]. This is later used to estimate

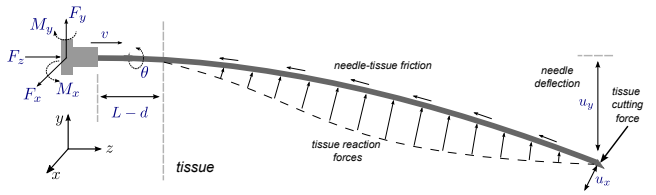

Fig. 2. Needle insertion in soft tissue. F_x, F_y are the forces measured at the needle base in the x and y direction, and F_z is the needle insertion force. M_x, M_y are the torques measured at the needle base around x and y respectively. The position of the needle tip in the (y,z) and (x,z) planes are denoted u_y and u_x.

needle insertion force F_z, a useful piece of information for haptic simulation purposes.

In addition to the insertion-specific parameters listed above, needle deflection also depends on the mechanical properties of the tissue [9, 15]. This information is difficult to obtain for heterogeneous or *in-vivo* tissues and as a consequence, heterogeneous tissue is in most instances assumed to be homogeneous [8], or approximated by a series of different local homogeneous models [12]. Instead of characterizing the tissue, and using this information as input, we rather consider the forces and torques acting at the needle base, which are directly related to tissue characteristics and to the magnitude and direction of needle deflection [20, 21].

Lateral forces at the needle base (F_x, F_y) : We demonstrated in our previous work that needle deflection can be calculated via forces measured at the needle base [21]. Considering the case of a needle modelled as a cantilever beam as shown in Fig. 2, the vertical and horizontal forces at the base, called F_x and F_y, are directly proportional to the in-plane and out-of-plane needle deflection, respectively. These forces represent the integral of all loads applied along the needle shaft combined with the projection of the needle-tissue cutting force along each plane.

Lateral moments at the needle base (M_x, M_y) : The moments measured at the needle base carry information about how the needle deforms the surrounding tissue during insertion since they depend on the distribution of the loads applied on the needle shaft, i.e., at which point along the shaft the resultant force F_x or F_y is applied. Hence, the torques also depend on the amount of needle deflection in each plane [21]. Note that the resultant force along x in Fig. 2 generates a torque M_y around the y axis, and the force F_y results in a torque M_x, measured around x.

In the next section, we will devise a model that treats the needle insertion procedure as a black box whose inputs can be the parameters listed above and whose outputs are the in-plane and out-of-plane needle deflections, and the needle insertion force.

B. Data-driven Modelling of Needle Deflection

Global modelling has traditionally been the approach taken to model needle deflection in soft tissue. This technique has proven to be a suitable solution for representing needle steering in homogeneous tissue where tissue parameters are assumed constant throughout the insertion process. In order to capture local variability in the properties of heterogeneous tissue, the approach presented here uses a memory-based model from process data and discretizes the process into several local linear models. This involves forming a database of several observations that describe the observed process input-output cause and effect. To approximate the nonlinear needle-tissue system with a set of relatively simple local models valid in a certain operating range, we will use the Just-In-Time (JIT) modelling approach [22, 23]. In the JIT model, when new input and output data are available, they are stored into a database. When estimation is required, the database samples are compared to the query and relevant samples located in a neighbourhood region around the query are selected. A local model is then constructed to estimate the output variables.

There are four main steps in the JIT model to predict the model output of a data query [17] (see Fig. 1):

1) The relevant data samples are selected according to some similarity criteria to the query;
2) Weights are assigned to each data sample depending on the degree of similarity;
3) A local model is built based on the relevant data and the weights;
4) The local model calculates the corresponding model for the current query.

After determining the model output, the local model is discarded and the process is repeated for upcoming query inputs. These steps will be detailed in the following subsections.

1) Historical Database: Suppose that a database consisting of N process data $(\mathbb{X}_i, \mathbb{Y}_i)$ with $1 \leq i \leq N$, $\mathbb{X}_i \in \mathbb{R}^n$, and $\mathbb{Y}_i \in \mathbb{R}^m$ is collected. The vector $\mathbb{X}_i$ consists of values of the process input(s) that led to the corresponding system output $\mathbb{Y}_i$. For the needle-tissue interaction environment, consider the input vector to be

$$\mathbb{X}_i = \begin{bmatrix} z_i & \theta_{1i} & \theta_{2i} & F_{xi} & M_{yi} & F_{yi} & M_{xi} & v_i \end{bmatrix} \quad (1)$$

where z is the needle insertion depth, θ_1 contains the distance from the current depth z to the depth at which the needle was first rotated axially by 180° and θ_2 contains the distance from the depth of second rotation. If needle rotation was not performed, then $\theta_1 = \theta_2 = 0$. If the needle was rotated at 20 mm, for instance, and the current depth is 45 mm, this implies $\theta_1 = 25$ mm. F_x and F_y are the forces measured at the needle base in the x and y directions shown in Fig. 2, and M_y and M_x are the resultant torques generated by F_x and F_z, respectively, measured around the y and x axes. Also, v in (1) is the needle insertion velocity.

The system output $\mathbb{Y}_i$ associated with $\mathbb{X}_i$ is

$$\mathbb{Y}_i = \begin{bmatrix} u_{xi} & u_{yi} & F_{zi} \end{bmatrix} \quad (2)$$

with u_x and u_y being the needle tip deflection in the (y,z) plane defined in Fig. 2 (or in-plane needle deflection), and the needle tip deflection in the (x,z) plane (or out-of-plane needle deflection), respectively, and F_z is the needle insertion force. Estimating the latter has many practical applications in haptic simulation of needle steering.

Given a specific data query $\mathbb{X}_q \in \mathbb{R}^n$, whose structure and elements are identical to those defined for $\mathbb{X}_i$, the objective

of the JIT model is to predict the model output $\hat{\mathbb{Y}}_q = f(\mathbb{X}_q)$ given the historical database $(\mathbb{X}_i, \mathbb{Y}_i)_{i=1-N}$.

Note that $f(\mathbb{X}_q)$ relates eight inputs to only three outputs. From the discussion in Section II-A, it is evident that certain elements in $\mathbb{X}$ do not affect all the elements in the output vector $\mathbb{Y}$. Hence, and for a reason that will become evident in the following discussion, the elements in $\mathbb{X}$ are gathered into four new vectors according to their influence on each of the output variables in $\mathbb{Y}$. The needle insertion and rotation depths heavy influence all the model outputs and therefore constitute a new variable p_s defined as:

$$p_s = \begin{bmatrix} z & \theta_1 & \theta_2 \end{bmatrix} \tag{3}$$

The force and torque that reflect the amount of needle deflection in the (z,y) plane are F_x and M_y. It is assumed that F_y and M_x only influence the deflection in the (z,x) plane and *vice-versa*. Hence, let us create the following new variables

$$\begin{aligned} p_x &= \begin{bmatrix} F_x & M_y \end{bmatrix} \\ p_y &= \begin{bmatrix} F_y & M_x \end{bmatrix} \end{aligned} \tag{4}$$

Finally, the needle insertion velocity is assumed to only influence the insertion force and hence:

$$p_v = \begin{bmatrix} v \end{bmatrix} \tag{5}$$

For simplicity, the indices i or q were omitted. Now it is possible to compare the query to each data point stored in the database. By considering multiple measures of similarity, i.e., with respect to position, force, torque, and velocity, the model performance can be improved [24]. This is the focus of the next subsection.

2) Similarity Criteria: One of the most common similarity measures between the query data $\mathbb{X}_q$ and every sample $\mathbb{X}_i$ in the entire database is the Euclidean distance. As the input vector has been split into four vectors, one can now specify four independent similarity measures. For the sake of clarity, we will refer to and define these similarity measures as:

Distance in space (d_{si}):

$$d_{si} = \sqrt{(p_{si} - p_{sq}) D_s (p_{si} - p_{sq})^T} \tag{6}$$

Similarity in in-plane (d_{yi}) and out-of-plane (d_{xi}) forces, respectively:

$$\begin{aligned} d_{yi} &= \sqrt{(p_{yi} - p_{yq}) D_y (p_{yi} - p_{yq})^T} \\ d_{xi} &= \sqrt{(p_{xi} - p_{xq}) D_x (p_{xi} - p_{xq})^T} \end{aligned} \tag{7}$$

Similarity of needle insertion velocity:

$$d_{vi} = \sqrt{(p_{vi} - p_{vq}) D_v (p_{vi} - p_{vq})^T}. \tag{8}$$

In the above similarity criteria, D is a positive definite diagonal matrix carrying pondering coefficients to evenly consider variables with large and small magnitude in the Euclidean distance. Otherwise, variables with large magnitude would dominate the similarity calculations. The chosen matrices D are given in (9).

The similarity between the query and a dataset is now quantified by the distance d_i: the smaller the distance the more similar a data sample is to the query. The next step before constructing the local model is to assign weights to every data sample according to their similarities.

$$\begin{aligned} D_s &= \begin{bmatrix} (\max|z_i|)^{-2} & 0 & 0 \\ 0 & (\max|\theta_{1i}|)^{-2} & 0 \\ 0 & 0 & (\max|\theta_{2i}|)^{-2} \end{bmatrix}, \\ D_y &= \begin{bmatrix} (\max|F_{yi}|)^{-2} & 0 \\ 0 & (\max|M_{xi}|)^{-2} \end{bmatrix}, \\ D_x &= \begin{bmatrix} (\max|F_{xi}|)^{-2} & 0 \\ 0 & \max(|M_{yi}|)^{-2} \end{bmatrix}, \\ D_v &= \max(|v_i|)^{-2}. \end{aligned} \tag{9}$$

3) Weighting Functions: Once the similarity of each database sample with respect to a given query is known, the next step is to assign weights to the database samples. Essentially, the weighting function takes the similarity measure as input and produces a non-negative weight for each sample as the output. Weighting the data can be interpreted as considering only relevant samples and discarding irrelevant ones. Thus, the output of weighting functions and the similarity measure must be proportional, i.e., the greater the similarity between samples the higher the weight assigned to a particular sample. A typical weighting function is the Gaussian kernel where the weight w_i assigned to the sample i is $w_i = e^{-d_i^2}$ where d_i is one of the similarity criteria calculated in (6-8) [25].

In this paper we propose a combination of different Gaussian kernels that will allow to assign different weights to every data sample depending on the considered output variable. For instance, we assume that the in-plane deflection is only a function of needle insertion depth and rotation profile (spatial similarity d_s), and in-plane forces, whose similarity is given by d_y. Hence, the weight assigned to the database for in-plane deflection, called w_{yi}, is a function of only the spatial and in-plane similarity and it is thereby defined as:

$$w_{yi} = \frac{e^{-\left(d_{si}^2 \phi_{sy} + d_{yi}^2 \phi_y\right)}}{\max\left(e^{-\left(d_{si}^2 \phi_{sy} + d_{yi}^2 \phi_y\right)}\right)} = \frac{e^{-d_{si}^2 \phi_{sy}}}{\max(e^{-d_{si}^2 \phi_{sy}})} \frac{e^{-d_{yi}^2 \phi_y}}{\max(e^{-d_{yi}^2 \phi_y})} \tag{10}$$

where $\phi_{sy} > 0$ and $\phi_y > 0$ are smoothing parameters that determine the bandwidth of the local model, i.e., how large the size of the subset of data used to build the local model is. A large ϕ (low bandwidth) leads the weights to fall off very sharply with increasing distance d while a small ϕ (high bandwidth) allows for a gradual decrease in weights, and hence a larger number of historical samples will be considered. Generally, for highly non-linear systems a weight function with a steep slope is preferred.

To calculate the out-of-plane deflection, only the spatial and the out-of-plane similarities are considered. In the same way, for the insertion force weights only the spatial and velocity similarities are considered. Thereby, one defines the out-of-

plane and velocity weights as:

$$w_{xi} = \frac{e^{-\left(d_{si}^2\phi_{sx}+d_{xi}^2\phi_x\right)}}{\max\left(e^{-\left(d_{si}^2\phi_{sx}+d_{xi}^2\phi_x\right)}\right)} = \frac{e^{-d_{si}^2\phi_{sx}}}{\max(e^{-d_{si}^2\phi_{sx}})}\frac{e^{-d_{xi}^2\phi_x}}{\max(e^{-d_{xi}^2\phi_x})}$$
$$w_{zi} = \frac{e^{-\left(d_{si}^2\phi_{sz}+d_{zi}^2\phi_z\right)}}{\max\left(e^{-\left(d_{si}^2\phi_{sz}+d_{zi}^2\phi_z\right)}\right)} = \frac{e^{-d_{si}^2\phi_{sz}}}{\max(e^{-d_{si}^2\phi_{sz}})}\frac{e^{-d_{zi}^2\phi_z}}{\max(e^{-d_{zi}^2\phi_z})} \tag{11}$$

in which ϕ_{sx}, ϕ_{sz}, ϕ_x and ϕ_z are smoothing parameters to be determined later by cross validation.

4) Locally Weighted Model Prediction: Knowing the relevance of every sample as quantified by the weights, a local model can be built for predicting the output. The idea of the local model is to approximate the non-linear behaviour of the needle in tissue by a set of simple local linear models that are only valid in a certain operating range upon query, allowing a simple structure to be chosen [16]. In this paper, we will use the weighted average model.

Consider the $3 \times N$ weight matrix W defined in (12) whose rows are formed by the N weights assigned to every data sample, and whose columns correspond to one of the three weights defined earlier for each of the three output variables.

$$W = \begin{bmatrix} w_{x1} & w_{x2} & \dots & w_{xN} \\ w_{y1} & w_{y2} & \dots & w_{yN} \\ w_{z1} & w_{z2} & \dots & w_{zN} \end{bmatrix} \tag{12}$$

Based on (2), consider also the $N \times 3$ matrix P formed by outputs of all data samples such that

$$P = \begin{bmatrix} \mathbb{Y}_1 \\ \mathbb{Y}_2 \\ \vdots \\ \mathbb{Y}_N \end{bmatrix} = \begin{bmatrix} u_{x1} & u_{y1} & F_{z1} \\ u_{x2} & u_{y2} & F_{z2} \\ & \vdots & \\ u_{xN} & u_{yN} & F_{zN} \end{bmatrix} \tag{13}$$

The estimated output for the query $\mathbb{X}_q$ is found by applying the weighted average prediction to all the database samples as:

$$\hat{y}_q = \begin{bmatrix} \hat{u}_x \\ \hat{u}_y \\ \hat{F}_z \end{bmatrix}^T = \begin{bmatrix} \frac{\sum_{j=1}^N W_{1j}P_{j1}}{\sum_{j=1}^N W_{1j}} & \frac{\sum_{j=1}^N W_{2j}P_{j1}}{\sum_{j=1}^N W_{2j}} & \frac{\sum_{j=1}^N W_{3j}P_{j3}}{\sum_{j=1}^N W_{3j}} \end{bmatrix} \tag{14}$$

where W_{ab} refers to the a^{th} row and b^{th} column of the matrix W. Once the input is updated, the model is discarded and this process is repeated around the new operating point.

III. Results

A. Data Collection

The 2 degrees-of-freedom (DOF) prismatic-revolute robotic system shown in Fig. 3(a) was used to perform needle insertion in *ex-vivo* heterogeneous tissue and to collect data. An 18-gauge, 200 mm long brachytherapy needle was connected to a 6-DOF force/torque sensor (JR3, Inc. Woodland, USA) that measures the torques and forces at the needle base. The torsional torque around the needle shaft was not considered. The force sensor and needle can be rotated axially by a geared DC motor in order to change the orientation of the needle bevel angle. The assembly slides on a linear stage that was manually translated towards tissue at different speeds while the needle can be automatically rotated at predefined insertion depths. In all the insertions, the bevel started at the same position facing up, so that the needle deflected downwards.

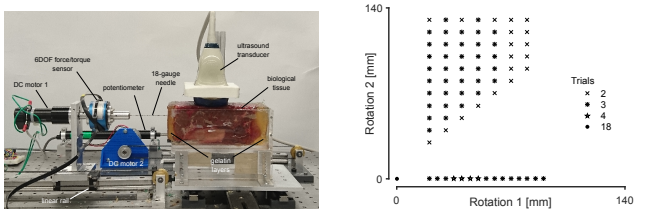

(a) Needle insertion device used for data collection (b) Depth of axial rotation for each trial

Fig. 3. The needle insertion robot used to perform needle insertion in *ex-vivo* tissue (a) and the distribution of the depth of needle rotation (b). The data base consists of 18 insertions without axial needle rotation, 49 insertions with single axial rotation, and 149 insertions with double axial rotation, totalling 216 needle insertion trials in 8 different *ex-vivo* tissue samples.

In order to track the position of the needle tip as it is inserted into tissue, a 4DL14-5/38 linear ultrasound transducer connected to a SonixTouch ultrasound machine (Ultrasonix, Richmond, Canada) moved on the tissue surface and acquired 2D images at 30 Hz of the needle in a plane perpendicular to the needle shaft (the plane (z,y) in Fig. 2), such that each transverse image contained a cross section of the needle. The ultrasound probe was connected to a second linear stage, whose horizontal position was measured by a linear potentiometer (Midori Precisions, Tokyo, Japan) and fedback into a PID controller that regulates the position of the ultrasound probe such that it followed the needle tip during insertion. From each ultrasound image, the coordinates of the needle tip and hence the in-plane and out-of-plane needle deflection were measured using the image processing method described in [7].

Needle insertion was performed in six different tissues samples, all prepared by embedding a piece of beef tenderloin in a mixture of 150 grams of industrial gelatin derived from acid-cured tissue (gel strength 300 from Sigma-Aldrich Corporation, Saint Louis, USA) per kilogram of water. Each tissue sample comprised three different layers as shown in Fig. 3(a). The needle was initially inserted through the 15-20 mm long layer of stiff gelatin that recreates a kin layer, before it reached the 100-110 mm long biological tissue layer. The biological tissue presented several layers of fat and muscle, making it highly heterogeneous. Once the needle tip exited the latter, it travelled through another 15-20 mm layer of gelatin. The maximum needle insertion depth was fixed to 140 mm in all *ex-vivo* experiments. On average, 35 needle insertions were performed in each tissue at different locations in order to avoid the influence of past insertions on the current one. Data was collected in a constant ambient temperature of 21°. As the needle was manually inserted, the needle base could be rotated axially by 180 degrees at up to two predefined insertion depths. The distribution of rotation depths is shown in Fig. 3(b). The number of trials performed in each scenario was randomly determined. In total, 18 insertions without axial needle rotation, 49 insertion with single axial rotation and

149 insertion with 2 axial needle rotations composed the final database. This amounted to a total of 216 needle insertions.

To form the data samples from each insertion, measurements were taken at increments of 0.56 mm in insertion depth, meaning that each needle insertion was discretized into 250 independent observations (data samples) equally spaced with respect to depth. Each observation therefore consisted of a $250 \times M$ input matrix where $M = 8$ is the number of measurements i.e., the needle insertion depth, the forces and torques at the needle base, the distance from the first and second depth of rotation, and the needle insertion velocity. Each sample also had a 250×3 output matrix containing the in-plane and out-of-plane deflection and the needle insertion force. All combined, the 216 observations formed an $54,000 \times 8$ input matrix and $54,000 \times 3$ output matrix that represent our database with $N = 54,000$ data samples. In the database, the samples were stored following the order of the observations from which they are taken. For instance, columns $1 \leq i \leq 249$ contain the samples that comprise the first insertion, columns $250 \leq i \leq 499$ contain the second one, and so on as follows

$$\mathbb{X} = \begin{bmatrix} z_1 & \theta_{1_1} & \theta_{2_1} & F_{x1} & M_{y1} & F_{y1} & M_{x1} & v_1 \\ z_2 & \theta_{1_2} & \theta_{2_2} & F_{x2} & M_{y2} & F_{y2} & M_{x2} & v_2 \\ & & & \vdots & \vdots & & & \\ z_{249} & \theta_{1_{249}} & \theta_{2_{249}} & F_{x249} & M_{y249} & F_{y249} & M_{x249} & v_{249} \\ z_{250} & \theta_{1_{250}} & \theta_{2_{250}} & F_{x250} & M_{y250} & F_{y250} & M_{x250} & v_{250} \\ & & & \vdots & \vdots & & & \\ z_{499} & \theta_{1_{499}} & \theta_{2_{499}} & F_{x499} & M_{y499} & F_{y499} & M_{x499} & v_{499} \\ & & & \vdots & \vdots & & & \\ z_N & \theta_{1_N} & \theta_{2_N} & F_{xN} & M_{yN} & F_{yN} & M_{xN} & v_N \end{bmatrix} \begin{matrix} \Big\} 1 \\ \\ \\ \Big\} 2 \\ \\ \\ \end{matrix}$$

$$\mathbb{Y} = \begin{bmatrix} u_{x1} & u_{x2} & \dots & u_{x249} & u_{x250} & \dots & u_{x499} & \dots & u_{xN} \\ u_{y1} & u_{y2} & \dots & u_{y249} & u_{y250} & \dots & u_{y499} & \dots & u_{yN} \\ F_{z1} & F_{z2} & \dots & F_{z249} & F_{z250} & \dots & F_{z499} & \dots & F_{zN} \end{bmatrix}^T .$$

insertion 1 (under $u_{x1} \dots F_{z249}$) insertion 2 (under $u_{x250} \dots F_{z499}$)

It is worth pointing out, however, that the modelling presented in this paper does not presuppose that the samples are stored in a sequential fashion, or sorted by needle insertion. In fact, each sample is an observation of the system at a particular instant in time. Therefore, they could be randomly placed in the database since every sample is treated as a single observation in time and is unrelated to the other ones.

B. Experimental Validation

To calibrate the model parameters in different case studies, i.e. to determine the bandwidth/smoothing parameters ϕ, k-fold cross-validation was performed [26, 27]. The database was divided into a training set and a validation set. The selected training set was partitioned into k equal sized sub-samples, each of which contained a complete needle insertion (250 samples). Of the k insertions in the training set, one subset of data was retained and used as query input for testing the model, and the remaining $n = k-1$ sub-sets formed the database. The process was then repeated k times, with each of the k insertions being used exactly once. The $Q = (k-1) \times 250$ absolute prediction errors for each model output from each of the folds were averaged to produce a single estimation for a given set of smoothing parameters ϕ_{sx}, ϕ_{sy}, ϕ_{sz}, ϕ_x, ϕ_y, and ϕ_z. The model predictions were discarded once the estimation was completed. Hence, the considered database had a fixed size and only contained points obtained from real measurements. The smoothing parameters were interactively updated in order to minimize the prediction error via Particle Swarm optimization [28].

Particle Swarm is a stochastic technique that optimizes a problem by iteratively trying to improve a candidate solution with regard to a cost function. A population of candidate solutions (particles) is randomly generated and moved around the search-space as a function of the position of each particle and the position of the best current solution known. The optimization consists of, at each time step, changing the velocity of each particle toward the best known position in the search space. The best solution is then updated in each time step, and the process is repeated exhaustively to bring the particles toward the optimal solution. In our case, the optimization process was executed three times, every time considering the prediction error of the model outputs. The absolute average error in predicting the model outputs is

$$\varepsilon = \frac{1}{Q} \sum_{j=1}^{Q} |\mathbb{Y}_j - \hat{y}_{qj}| \tag{15}$$

where Q is the number of evaluated query inputs in a particular scenario, $\hat{y}_{qj}$ is the estimated output vector and $\mathbb{Y}_j$ is the actual value of the output vector of the query $1 \leq j \leq Q$.

The accuracy of the proposed sensor was validated in five different Case studies.

Case 1 to 3 : One out of three needle insertions was removed from the database to be used as a query. Cross validation was performed in the remaining data points using the method described above. Hence, the database was composed of 36,000 points and validation was performed with 18,000 samples. In each of the three Cases, a new set of insertions was used as queries.

An example of the iterative search to find the model parameters for in-plane deflection is shown in Fig. 4. This process was repeated for our-of-plane deflection estimation and insertion force estimation. Using the optimal parameters, an example of the weights assigned to the data samples for a random query is shown in Fig. 5(a). The query has $z_q = 65$ mm, $\theta_{q1} = 45$ mm and $\theta_{q2} = 0$, which means that it stems from an insertion with a current insertion depth of 65 mm, and with an axial rotation performed at $65 - 45 = 20$ mm. The upper panel of Fig. 5(a) shows the weights attributed to samples according to their spatial similarity to the query (the first fraction in (10) or w_{yi} for $\phi_y = 0$). For clarity, only the closest 16,000 samples are displayed. For the current query, samples from insertions with first axial rotations at approximately 20 mm and without second rotations received high weights. Notice that each of the vertical bars in the panel is in fact a Gaussian curve centred at the current depth for each of the relevant insertions (see the zoomed area in the first panel). In the second panel, the weights assigned to the samples considering only out-of-plane forces are shown. The final weights given to the samples for out-of-plane deflection can be seen in the third panel, which

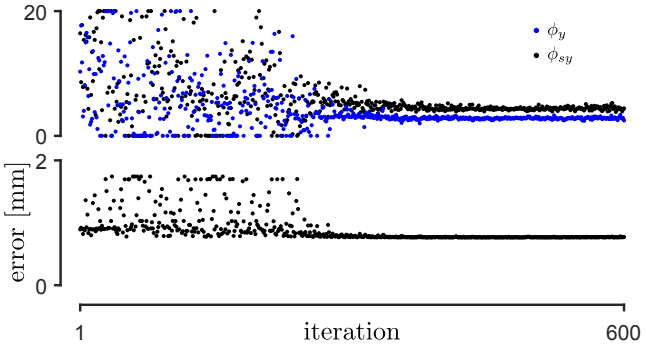

Fig. 4. Iterative search for the smoothing parameters ϕ_y and ϕ_{sy} during cross validation via Particle Swarm optimization. The error is defined as the average absolute difference between measured and estimated in-plane deflections.

is obtained by multiplying the former values.

When several successive query points are combined and input in the model, the deflection of the needle tip and the insertion force for a complete needle deflection can be estimated as shown in Fig. 5(b). The average error in predicting the in-plane and out-of-plane needle deflection, and the insertion force as a function of the insertion depth, is shown in Fig. 5(c) and 5(d) for all 72 insertion queries in Case 1. The average error did not exceed 1.7 mm for the in-plane deflection, 1.9 mm for the out-of-plane deflection, and 0.8 N for the insertion force. Table I summarizes the model accuracy in four different scenarios considering: 1) all insertions combined, 2) only insertions without axial needle rotation, and insertions with 3) one, and 4) two axial rotations. The size of the database, the number of evaluated queries, and the smoothing parameters for each experimental Case are presented in Table II.

Case 4 : Two out of three needle insertions were removed from the database and used as queries after cross validation of the model using the remaining samples. As a result, the database was composed of 72 needle insertions (18,000 samples) and 144 insertions (36,000 queries) were evaluated.

The average estimation error for the first four cases is presented in Fig. 6. The maximum deflection and insertion force estimation error did not exceed 2 mm and 0.8 N respectively.

Case 5 is the result of the cross validation considering the whole database as the training set. This Case demonstrates the best performance of the model, achieved with a database large enough to reject the effects of outliers and represent all the steering cases (rotation depths) that the inputs can have.

Cases 1b to 3b employed the same queries and training samples as Cases 1 to 3, respectively, but do not consider the input forces/torques and velocity as model input. K-fold optimization was performed considering $\phi_x = \phi_y = \phi_z = 0$. This demonstrates the influence of the additional measurements on model accuracy.

Table I summarizes the average absolute estimation errors for all the Case studies, the number of samples in the database N, the number of evaluated queries Q, as well as the smoothing parameters calculated for each training set. If torques/forces and velocity were not used, the overall model accuracy was reduced by 18%.

IV. Discussion

The performance of the proposed soft sensor was evaluated in five different Case studies. The average absolute error in predicting the in-plane and out-of-plane deflection does not exceed 2 mm and the insertion force can be estimated with an average accuracy of 0.5 N. From the experimental results, some recommendations for implementing a JIT based soft sensor can be drawn:

Recommendation 1: The model performance heavily depends on the size of the database. Although it is difficult to determine a minimum size for the database, the samples should comprise all the scenarios that the query might take, i.e., rotation depths and similar tissue properties. The most important factor influencing needle deflection is the depth at which the needle is rotated. We observed through simulations and experimentally that the database should contain samples having rotations in a range of at most 10 mm from the one specified in the query. In addition, another factor that influences the model output is the number of trials for a given needle insertion profile, which should be representative enough to capture experimental variability of the process output. Thus, the number of data samples would have a Gaussian distribution centred around the most common rotation depth in the queries.

Recommendation 2: The computation time linearly increases with the number of samples in the database. In order to optimize the computation time, each needle insertion can be discretized with a lower spatial resolution depending on the application and requirements. If estimation of needle deflection is only required for certain insertion depths, predictions can be made around the desired depth considering only neighbouring samples.

Recommendation 3: Despite using a weighted average for model prediction, outliers can affect prediction accuracy and therefore must be removed from the database, or alternatively the database should be large enough to reject the influence of outliers as demonstrated in Case 5.

Recommendation 4: In order to minimize invasive preoperative interventions, data collection can be based on a physical model of needle steering that calculates the optimal rotation depths. Each insertion can then be stored in the database and the rotation depth updated from trial to trial.

Recommendation 5: The JIT model cannot be used to extrapolate the predictions beyond the scenarios known in the database. This infers that tissues with different Young's moduli can be used as long as other insertions in tissues having similar characteristics are available.

In contrast to model-based estimation of needle deflection, the approach introduced in this paper requires a large database containing observation of needle deflection for a variety of steering actions, which may be difficult to obtain in a clinical scene. The obtained accuracy using the JIT model is about 1.25 mm, which is lower than the accuracy we obtained through model-based estimation of needle deflection previously presented in [3, 13, 20, 21], where we reported an accuracy of about 1 mm. However, it is important to note that the model based estimation does not hold for highly heterogeneous tissue such as those considered in this paper. Therefore, the JIT

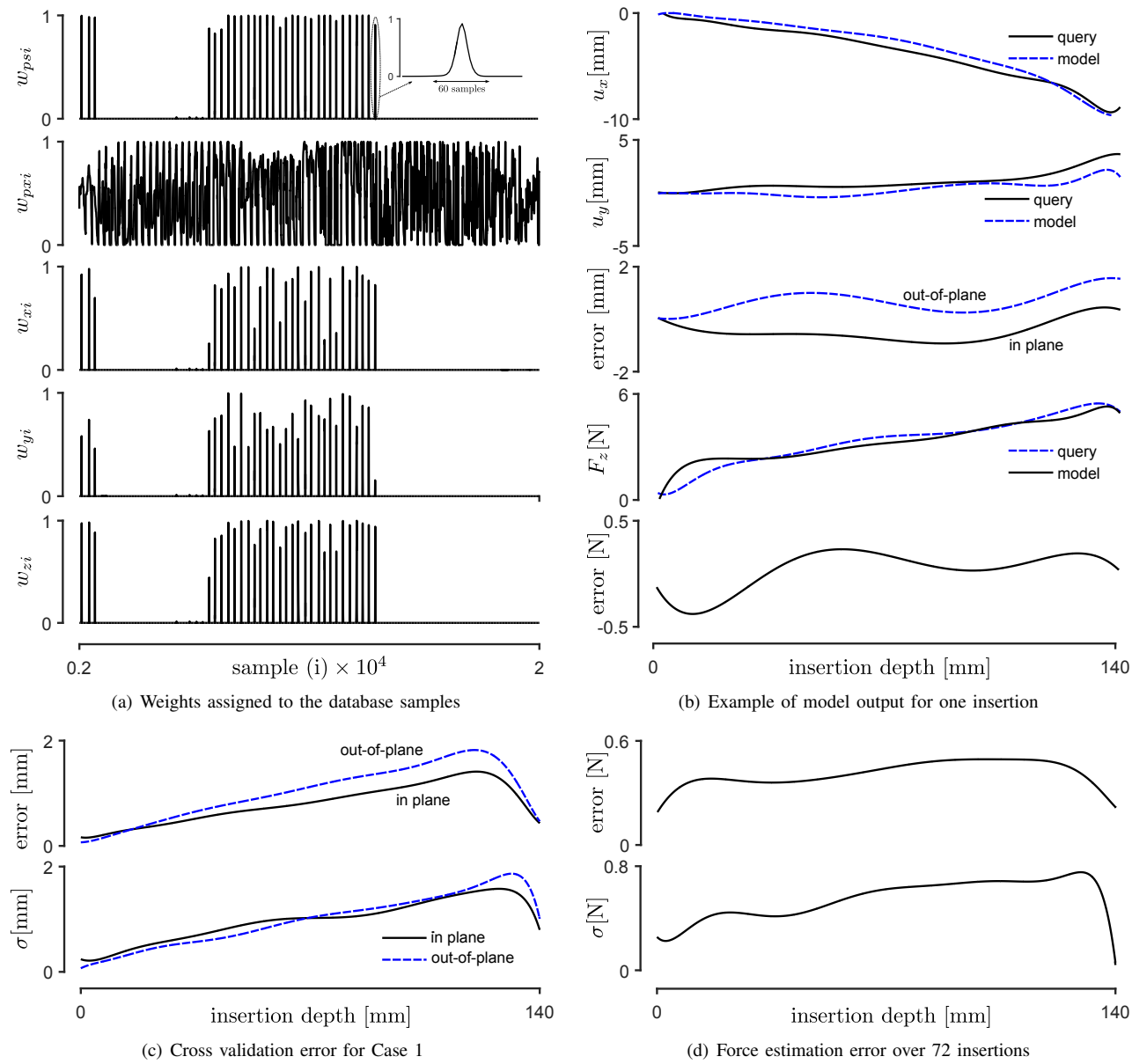

(a) Weights assigned to the database samples

(b) Example of model output for one insertion

(c) Cross validation error for Case 1

(d) Force estimation error over 72 insertions

Fig. 5. Example of cross validation results. 5(a) shows the weights assigned to all data samples for a given query. In 5(b), a complete needle insertion is evaluated using 250 successive samples. The average error and standard deviation σ in predicting the needle tip deflection and insertion force for 72 needle insertions are presented in 5(c) and 5(d), respectively, for Case 1 only.

provides a good alternative to model based estimation while maintaining a relatively good accuracy.

A. Potential Applications

The proposed application of the data-driven model is in developing a soft sensor for needle deflection and insertion force. Considering the entire database of 54,000 samples, in a computer equipped with a 3.2 GHz Intel Core i7-3930K CPU and 14 GB of RAM, a query is processed in 13 milliseconds. This makes such a soft sensor suitable for real time application with 50% higher sampling rate compared to 2D ultrasound images. Another advantage of this approach is that it only requires a force/torque sensor and a means of measuring the needle insertion depth and rotation angle, making it cost effective compared to other sensors such as those based on optical fibres, electromagnetic tracking, ultrasound images, and X-Ray.

The database and the estimated output of a given query can be employed to update, in real time, the parameters of a needle steering controller such as those depending on the local properties of tissue. Data mining analytic processes can be implemented to explore the database in search of systematic relationships between needle curvature and tissue stiffness, or tissue cutting force and forces at the needle base, etc. Hence, when associated with a needle-tissue interaction model, the needle deflection further along the insertion process can also be estimated based on the current observations.

Another direct application of the data-driven model can be found in developing haptic simulators for skills assessment and

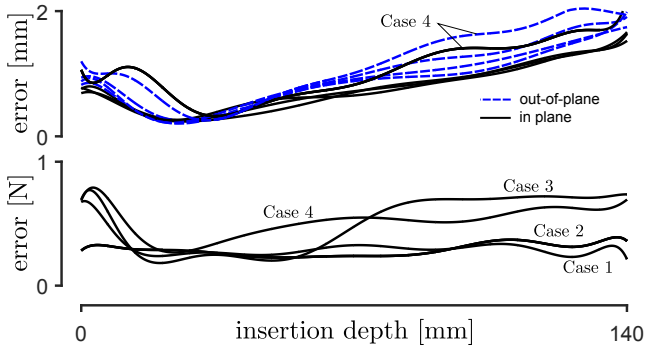

Fig. 6. Average absolute error in predicting needle tip deflection and insertion forces for Cases 1 to 4.

TABLE I
AVERAGE PREDICTION ERROR AND STANDARD DEVIATION

Scenario		in-plane error [mm]	out-of-plane error [mm]	insertion force error [N]
Case 1	All insertions	0.81 ±0.41	1.28 ± 0.84	0.45 ± 0.07
	No rotation	0.85 ±0.55	1.58 ± 0.92	0.36 ± 0.06
	1 rotation	1.02 ±0.53	1.28 ± 0.78	0.55 ± 0.07
	2 rotations	0.64 ±0.39	0.88 ± 0.51	0.40 ± 0.05
Case 2	All insertions	0.81 ±0.37	1.26 ± 0.60	0.42 ± 0.04
	No rotation	0.59 ±0.25	2.21 ± 1.12	0.41 ± 0.06
	1 rotation	1.05 ±0.51	1.32 ± 0.80	0.48 ± 0.09
	2 rotations	0.66 ±0.36	0.94 ± 0.61	0.38 ± 0.04
Case 3	All insertions	0.81 ±0.36	1.13 ± 0.55	0.52 ± 0.08
	No rotation	0.65 ±0.41	1.32± 0.61	0.50 ± 0.01
	1 rotation	0.97 ±0.43	1.19± 0.85	0.52 ± 0.01
	2 rotations	0.78 ±0.39	1.07 ± 0.59	0.52 ± 0.01
Case 4	All insertions	0.94 ±0.51	1.27 ± 0.55	0.42 ± 0.04
	No rotation	0.77 ±0.37	1.86± 1.24	0.36 ± 0.10
	1 rotation	1.55±0.71	1.69 ± 0.51	0.48 ± 0.08
	2 rotations	0.83±0.42	1.07 ± 0.58	0.41 ± 0.06
Case 5	All insertions	0.79 ±0.36	1.21 ± 0.60	0.46 ± 0.05
	No rotation	0.77 ±0.41	1.58 ± 0.92	0.38 ± 0.08
	1 rotation	0.77 ±0.37	1.05 ± 0.55	0.31 ± 0.06
	2 rotations	0.59 ±0.32	0.78 ± 0.46	0.35 ± 0.05
Case 1b	All insertions	0.86±0.46	1.67± 0.34	0.46 ± 0.05
	No rotation	0.96 ±0.46	1.89 ± 1.00	0.36± 0.08
	1 rotation	1.03±0.62	1.45 ± 0.99	0.60 ± 0.02
	2 rotations	0.75 ±0.44	1.07 ± 0.60	0.42 ± 0.05
Case 2b	All insertions	0.98 ±0.49	1.38 ± 0.71	0.51 ± 0.05
	No rotation	0.65 ±0.24	2.42 ± 1.30	0.45 ± 0.06
	1 rotation	1.33 ±0.69	1.52 ± 0.93	0.58 ± 0.12
	2 rotations	0.88±0.52	1.08 ± 1.21	0.41 ± 0.06
Case 3b	All insertions	0.99 ±0.38	1.21 ± 0.57	0.53 ± 0.10
	No rotation	0.67 ±0.37	1.67 ± 0.82	0.51 ± 0.12
	1 rotation	1.50±0.83	1.42 ± 0.78	0.52 ± 0.10
	2 rotations	0.83±0.45	1.10 ± 0.57	0.54 ± 0.14

development in needle insertion procedures. As demonstrated in the experimental results, the model estimates the 3D needle deflection and the needle insertion force. In a haptic trainer, the user can receive quantifiable performance assessments in terms of current and future needle tip positioning errors according to different sets of steering manoeuvres, while receiving real-time haptic feedback of the insertion force. Such a system has the potential to inform a physician at an experiential, hands-on level regarding the mechanics at play in needle insertion, which can greatly help reduce the clinical learning curve in

TABLE II
DATABASE SIZE, NUMBER OF EVALUATED SAMPLES, AND SMOOTHING PARAMETERS FOR EACH EXPERIMENTAL CASE.

	database size N	number of evaluated queries Q all	0 rotation	1 rotation	2 rotations
Cases 1 to 3	36,000	18,000	1,750	4,000	12,250
Case 4	18,000	36,000	3,500	8,000	24,500
Case 5	53,750	54,000	4,500	12,250	37,250

	ϕ_{xs}	ϕ_x	ϕ_{ys}	ϕ_y	ϕ_{sz}	ϕ_z
Case 1	13.88	8.15	11.75	19.5	20.0	19.89
Case 2	18.24	7.85	6.71	15.51	3.88	6.16
Case 3	4.60	2.88	5.74	20.25	4.42	2.22
Case 4	7.40	4.13	5.21	5.94	3.62	19.58
Case 5	6.50	10.0	7.62	9.50	4.21	3.00
Case 1b	9.42	0.00	9.52	0.00	10.22	0.00
Case 2b	22.50	0.00	9.34	0.00	15.60	0.00
Case 3b	5.69	0.00	6.00	0.00	8.63	0.00

applications such as brachytherapy, microwave ablation, drug administration and other minimally invasive procedures [29].

V. CONCLUSION

In this paper a novel method for estimating needle deflection in heterogeneous tissue is proposed. Readings of a force/-torque sensor connected at the needle base and information of insertion depth and needle rotation profiles are the only input to the data-driven model. The needle insertion process is broken down into small multiple regions corresponding to an observation of the needle-tissue states at a particular instant in time. Several observations are combined in order to form a database that is scanned every time a new query arrives. A modified variation of the Just-in-Time (JIT) learning method allows for selecting the subset of historical data that is most relevant to the query according to two independent similarity criteria for each output variable i.e., the insertion specific parameters (insertion depth and needle rotation) and the needle-tissue specific parameters (reaction forces and torques). Once the subset of data is selected, a local linear model is fit to the selected points and the system output can be determined. Thereby, local non-linearities and other uncertainties present in the needle-tissue interaction can be captured.

The model outputs the in-plane and out-of-plane needle tip deflection along with the needle insertion force. The former has many practical applications in providing real-time feedback for needle steering controllers or visual feedback to the surgeon performing needle insertion. The latter has direct applications in developing haptic simulator for skills assessment and development in needle-based intervention.

Overall, the average prediction error for needle deflection in-plane and out-of-plane does not exceed 2 mm, which is in the range of the smallest tumour that can be detected in ultrasound images. The accuracy and the high sampling rate make the sensor suitable for real time measurements of needle deflection.

REFERENCES

[1] A. M. Okamura, C. Simone, and M. Leary, "Force modeling for needle insertion into soft tissue," *Biomedical*

Engineering, IEEE Transactions on, vol. 51, no. 10, pp. 1707–1716, 2004.

[2] N. Abolhassani, R. Patel, and M. Moallem, "Needle insertion into soft tissue: A survey," *Medical engineering & physics*, vol. 29, no. 4, pp. 413–431, 2007.

[3] M. Khadem, C. Rossa, N. Usmani, R. S. Sloboda, and M. Tavakoli, "A two-body rigid/flexible model of needle steering dynamics in soft tissue," *IEEE/ASME Transactions on Mechatronics*, vol. 21, no. 5, pp. 2352–2364, Oct 2016.

[4] C. Rossa, M. Khadem, R. Sloboda, N. Usmani, and M. Tavakoli, "Constrained optimal control of needle deflection for semi-manual steering," in *2016 IEEE International Conference on Advanced Intelligent Mechatronics (AIM)*, July 2016, pp. 1198–1203.

[5] B. Dobler, S. Mai, C. Ross, D. Wolff, H. Wertz, F. Lohr, and F. Wenz, "Evaluation of possible prostate displacement induced by pressure applied during transabdominal ultrasound image acquisition," *Strahlentherapie und Onkologie*, vol. 182, no. 4, pp. 240–246, 2006.

[6] R. J. Webster, J. S. Kim, N. J. Cowan, G. S. Chirikjian, and A. M. Okamura, "Nonholonomic modeling of needle steering," *The International Journal of Robotics Research*, vol. 25, no. 5-6, pp. 509–525, 2006.

[7] M. Waine, C. Rossa, R. Sloboda, N. Usmani, and M. Tavakoli, "Needle tracking and deflection prediction for robot-assisted needle insertion using 2D ultrasound images," *Journal of Medical Robotics Research*, vol. 01, no. 01, p. 1640001, 2016.

[8] S. P. DiMaio and S. E. Salcudean, "Needle insertion modeling and simulation," *IEEE Transactions on Robotics and Automation*, vol. 19, no. 5, pp. 864–875, Oct 2003.

[9] M. Khadem, C. Rossa, R. S. Sloboda, N. Usmani, and M. Tavakoli, "Ultrasound-guided model predictive control of needle steering in biological tissue," *Journal of Medical Robotics Research*, vol. 01, no. 01, p. 1640007, 2016.

[10] O. Goksel, S. E. Salcudean, and S. P. Dimaio, "3D simulation of needle-tissue interaction with application to prostate brachytherapy," *Computer Aided Surgery*, vol. 11, no. 6, pp. 279–288, 2006.

[11] F. S. Azar, D. N. Metaxas, and M. D. Schnall, "A deformable finite element model of the breast for predicting mechanical deformations under external perturbations," *Academic Radiology*, vol. 8, no. 10, pp. 965–975, 2001.

[12] H. Lee and J. Kim, "Estimation of flexible needle deflection in layered soft tissues with different elastic moduli," *Medical & biological engineering & computing*, vol. 52, no. 9, pp. 729–740, 2014.

[13] C. Rossa, M. Khadem, R. Sloboda, N. Usmani, and M. Tavakoli, "Adaptive quasi-static modelling of needle deflection during steering in soft tissue," *IEEE Robotics and Automation Letters*, vol. 1, no. 2, pp. 916–923, July 2016.

[14] C. Rossa, N. Usmani, R. Sloboda, and M. Tavakoli, "A hand-held assistant for semi-automated percutaneous needle steering," *IEEE Transactions on Biomedical Engineering*, vol. In press, 2016.

[15] P. Moreira and S. Misra, "Biomechanics-based curvature estimation for ultrasound-guided flexible needle steering in biological tissues," *Annals of biomedical engineering*, vol. 43, no. 8, pp. 1716–1726, 2015.

[16] C. Cheng and M.-S. Chiu, "A new data-based methodology for nonlinear process modeling," *Chemical Engineering Science*, vol. 59, no. 13, pp. 2801–2810, 2004.

[17] F. P. Vidal, N. W. John, A. E. Healey, and D. A. Gould, "Simulation of ultrasound guided needle puncture using patient specific data with 3D textures and volume haptics," *Computer Animation and Virtual Worlds*, vol. 19, no. 2, pp. 111–127, 2008.

[18] C. Rossa, R. Sloboda, N. Usmani, and M. Tavakoli, "Estimating needle tip deflection in biological tissue from a single transverse ultrasound image: application to brachytherapy," *International Journal of Computer Assisted Radiology and Surgery*, vol. 11, no. 7, pp. 1347–1359, 2016.

[19] M. Waine, C. Rossa, R. Sloboda, N. Usmani, and M. Tavakoli, "3D needle shape estimation in TRUS-guided prostate brachytherapy using 2D ultrasound images," *IEEE Journal of Biomedical and Health Informatics*, vol. PP, no. 99, pp. 1–1, 2015.

[20] M. Khadem, C. Rossa, R. S. Sloboda, N. Usmani, and M. Tavakoli, "Mechanics of tissue cutting during needle insertion in biological tissue," *IEEE Robotics and Automation Letters*, vol. 1, no. 2, pp. 800–807, July 2016.

[21] T. Lehmann, C. Rossa, N. Usmani, R. Sloboda, and M. Tavakoli, "A real-time estimator for needle deflection during insertion into soft tissue based on adaptive modeling of needle-tissue interactions," *IEEE/ASME Transactions on Mechatronics*, vol. In press, 2016.

[22] A. Singhal and D. E. Seborg, "Pattern matching in multivariate time series databases using a moving-window approach," *Industrial & engineering chemistry research*, vol. 41, no. 16, pp. 3822–3838, 2002.

[23] S. Yoon and J. F. MacGregor, "Fault diagnosis with multivariate statistical models part I: using steady state fault signatures," *Journal of process control*, vol. 11, no. 4, pp. 387–400, 2001.

[24] H. Wang and J. Yuan, "Collaborative multifeature fusion for transductive spectral learning," *IEEE Transactions on Cybernetics*, vol. 45, no. 3, pp. 451–461, March 2015.

[25] C. G. Atkeson, A. W. Moore, and S. Schaal, "Locally weighted learning for control," in *Lazy learning*. Springer, 1997, pp. 75–113.

[26] Y. Bengio and Y. Grandvalet, "No unbiased estimator of the variance of k-fold cross-validation," *The Journal of Machine Learning Research*, vol. 5, pp. 1089–1105, 2004.

[27] J. Shao, "Linear model selection by cross-validation," *Journal of the American statistical Association*, vol. 88, no. 422, pp. 486–494, 1993.

[28] R. C. Eberhart, J. Kennedy *et al.*, "A new optimizer using particle swarm theory," in *Proceedings of the sixth international symposium on micro machine and human science*, vol. 1. New York, NY, 1995, pp. 39–43.

[29] J. Rosen, B. Hannaford, C. G. Richards, and M. N. Sinanan, "Markov modeling of minimally invasive surgery based on tool/tissue interaction and force/torque signatures for evaluating surgical skills," *Biomedical Engineering, IEEE Transactions on*, vol. 48, no. 5, pp. 579–591, 2001.